

**Thermodynamics of bcc metals in phase-field-crystal models**A. Jaatinen,<sup>1,2</sup> C. V. Achim,<sup>1</sup> K. R. Elder,<sup>3</sup> and T. Ala-Nissila<sup>1,4</sup><sup>1</sup>*Department of Applied Physics, COMP Center of Excellence, Helsinki University of Technology, P.O. Box 1100, Helsinki FIN-02015 TKK, Finland*<sup>2</sup>*Department of Materials Science and Engineering, Helsinki University of Technology, P.O. Box 6200, Helsinki FIN-02015 TKK, Finland*<sup>3</sup>*Department of Physics, Oakland University, Rochester, Michigan 48309-4487, USA*<sup>4</sup>*Department of Physics, Brown University, Providence, Rhode Island 02912-1843, USA*

(Received 30 April 2009; revised manuscript received 16 July 2009; published 9 September 2009)

We examine the influence of different forms of the free-energy functionals used in the phase-field-crystal (PFC) model, and compare them with the second-order density-functional theory (DFT) of freezing, by using bcc iron as an example case. We show that there are large differences between the PFC and the DFT and it is difficult to obtain reasonable parameters for existing PFC models directly from the DFT. Therefore, we propose a way of expanding the correlation function in terms of gradients that allows us to incorporate the bulk modulus of the liquid as an additional parameter in the theory. We show that this functional reproduces reasonable values for both bulk and surface properties of bcc iron, and therefore it should be useful in modeling bcc materials. As a further demonstration, we also calculate the grain boundary energy as a function of misorientation for a symmetric tilt boundary close to the melting transition.

DOI: [10.1103/PhysRevE.80.031602](https://doi.org/10.1103/PhysRevE.80.031602)

PACS number(s): 81.10.-h, 61.50.Ah, 61.72.Bb, 61.72.Mm

**I. INTRODUCTION**

Many macroscopic material properties are strongly influenced by the complex spatial patterns that form on microscopic length scales during nonequilibrium processing. Such microstructures can include, for example, grain boundaries, antiphase domain walls, magnetic domains, and composition gradients. While these structures are not equilibrium states, their lifetimes can often be months, years, decades, or even longer and consequently they play a major role in determining real material properties. The precise nature of such microstructures can be controlled by the processing (solidification, ball milling, annealing, etc.) used to produce the material.

Despite the need for understanding the nonequilibrium processing routes that lead to microstructures that optimize material behavior, it has proved extremely difficult to accurately model microstructure formation. What makes modeling microstructure formation difficult is the emergence of different time and length scales in the problem, e.g., grain boundary formation takes place on the atomic length scale, while solute transport occurs on diffusive time and length scales. In most cases, molecular dynamics (MD) simulations with present-day computers are limited to time and length scales that are orders of magnitude smaller than needed to match experimental conditions. This limitation necessitates the development of coarse-grained methods for modeling microstructure formation.

One such method is the so-called phase-field-crystal (PFC) method [1], which models a field in the solid phase that exhibits the periodic nature of the underlying crystal lattice. The advantage of using this approach instead of spatially uniform or slow-varying phase fields is that many crystal-structure-related properties, e.g., multiple grain orientations, dislocations, and anisotropy, naturally arise in this model. On the downside, spatial grid resolution in PFC needs to be subatomic, thus making it challenging to reach the

length scales accessible by conventional phase-field approaches.

One obvious interpretation of the periodic order-parameter field used in the PFC model is that of a nonequilibrium ensemble average of the atomic number density. This interpretation makes it tempting to derive this phenomenological model from a microscopic theory. To this end, a connection between the PFC model and the classical density-functional theory (DFT) of freezing [2] was recently established by Elder *et al.* in Ref. [3]. In essence, it was shown that the free-energy functional used in earlier PFC studies can be obtained from the DFT of freezing by making certain approximations to the original functional. Unfortunately, the approximations are quite drastic and the PFC free-energy functional is not an accurate description of the original DFT. While it is possible in principle to directly use DFT to describe microstructure formation, in practice this turns out to be a very difficult task. The reason for this is that DFT predicts very sharp density peaks that require an extremely small spatial grid spacing as compared to the PFC density maxima, which are much smoother and easier to handle numerically.

In this paper we investigate several recently proposed approaches for selecting the PFC parameters to fit several macroscopic or thermodynamic features. More specifically, we examine the predictions for the fitting schemes proposed by Elder *et al.* [3] and Wu and Karma (WK) [4] and compare them with DFT results. As our main result we present a fitting procedure, containing one more parameter, which captures additional macroscopic features not included in the prior fits. We demonstrate that the model gives a relatively good description of many of the bulk and surface properties of bcc iron. The model is further used to estimate the grain boundary energy near the melting point of bcc iron at a specific density and temperature.

This paper is organized as follows. In Sec. II we briefly review the oldest and simplest version of the DFT of freezing and the methodology of PFC modeling, with the emphasis on

its connection to the DFT. These models are then applied to Fe and used to predict both bulk thermodynamics and surface properties in Sec. III. These calculations highlight the strengths and the weaknesses of the two different approaches. Finally, this information is exploited to develop a free-energy functional that maintains the computational simplicity of the PFC formulation yet provides better predictions for bulk and surface properties of bcc iron.

## II. THEORY

The PFC model is a method for modeling periodic systems, and it has already been applied to many different problems in materials science. Originally, the model was phenomenologically postulated in the spirit of Ginzburg-Landau (GL) theory by Elder *et al.* [1] in which the dynamics of the number density field ( $\rho$ ) was assumed to be dissipative and driven to minimize a free-energy functional. The rationale for proposing the free-energy functional was that it should be minimized when  $\rho$  forms a periodic structure as occurs in crystalline phases. Perhaps the simplest free-energy functional that has this feature was derived by Swift and Hohenberg [5] for Rayleigh-Bénard convection and it can be written as

$$F[\phi(\mathbf{r})] = \int d\mathbf{r} \left\{ \frac{1}{2} \phi(\mathbf{r}) [\alpha + \lambda(q_0^2 + \nabla^2)^2] \phi(\mathbf{r}) + \frac{g}{4} \phi(\mathbf{r})^4 \right\}, \quad (1)$$

where  $\phi(\mathbf{r})$  is a conserved order-parameter field related to the number density field and  $\alpha$ ,  $\lambda$ ,  $q_0$ , and  $g$  are phenomenological constants [1]. To model nonequilibrium phenomena, one also needs an equation of motion for the order-parameter field  $\phi(\mathbf{r})$ . As with most phase-field models for conserved fields, the dynamics are assumed to be dissipative, conserved, and driven to minimize the free energy in the usual manner, i.e.,

$$\frac{\partial \phi}{\partial t} = M \nabla^2 \frac{\delta F}{\delta \phi}, \quad (2)$$

where  $M$  is a mobility parameter. In the present work, however, no dynamical processes are considered.

The justification for functional (1) is the fact that for a certain parameter range, it is minimized by a periodic field corresponding to the bcc solid phase in three dimensions, while at some other parameter range the free energy is minimized by a uniform field corresponding to the liquid phase. In the model, the bcc structure always has a lower free energy than other structures such as the much more common fcc structure (see [4] for the full phase diagram). It is tempting to use Eq. (1) for modeling bcc materials because it has been shown to reproduce many crystal-structure-related properties of real materials, and it is fairly simple to use. The central issue here is how to choose the phenomenological parameters to model a specific material. To address this question, it is useful to consider the classical DFT of freezing.

The classical DFT of freezing is the statistical-mechanical theory of classical inhomogeneous fluids applied to the freezing transition. This approach to modeling the freezing

transition was pioneered by Ramakrishnan and Yussouff in the late 1970s [6]. A key component in this theory is the intrinsic Helmholtz free energy  $\mathcal{F}$ , which is a unique functional of the one-particle number density field  $\rho(\mathbf{r})$ . The interpretation of this functional is that, for any given density field, the functional derivative  $\delta \mathcal{F} / \delta \rho(\mathbf{r})$  equals the intrinsic chemical potential which gives rise to the given density field [7].

For an ideal gas, the intrinsic free energy is known exactly as

$$\mathcal{F}_{id} = k_B T \int d\mathbf{r} \rho(\mathbf{r}) [\ln(\rho(\mathbf{r}) \lambda_T^3) - 1], \quad (3)$$

where  $\lambda_T$  is thermal de Broglie wavelength. For an interacting system, however, calculating  $\mathcal{F}$  exactly requires calculating the partition function. To approximate the functional, one first writes  $\mathcal{F}$  as

$$\mathcal{F} = \mathcal{F}_{id} + \mathcal{F}_{xs}, \quad (4)$$

where  $\mathcal{F}_{id}$  is given by Eq. (3) and  $\mathcal{F}_{xs}$  is the contribution to  $\mathcal{F}$  from the interactions between particles.

Many different approximations to  $\mathcal{F}_{xs}$  have been proposed in the literature. We present here the simplest way to come up with a nonlocal expression for  $\mathcal{F}_{xs}$ , which is often referred to as the second-order theory. Knowing that  $\mathcal{F}_{xs}$  acts as a generating functional for the family of direct correlation functions,

$$\beta \frac{\delta^n \mathcal{F}_{xs}[\rho]}{\delta \rho(\mathbf{r}_1) \cdots \delta \rho(\mathbf{r}_n)} = -c^{(n)}(\mathbf{r}_1, \dots, \mathbf{r}_n; [\rho]), \quad (5)$$

we expand it to the second order around a uniform reference density  $\rho_0$ , leading to

$$\begin{aligned} \frac{\Delta \mathcal{F}}{k_B T} = & \int d\mathbf{r} \{ \rho(\mathbf{r}) \ln[\rho(\mathbf{r})/\rho_0] - \Delta \rho(\mathbf{r}) \} + \beta \mu_0 \int d\mathbf{r} \Delta \rho(\mathbf{r}) \\ & - \frac{1}{2} \int \int d\mathbf{r}_1 d\mathbf{r}_2 \Delta \rho(\mathbf{r}_1) c^{(2)}(\mathbf{r}_1, \mathbf{r}_2, \rho_0) \Delta \rho(\mathbf{r}_2), \end{aligned} \quad (6)$$

where  $\Delta \mathcal{F} = \mathcal{F}[\rho] - \mathcal{F}[\rho_0]$ ,  $\Delta \rho(\mathbf{r}) = \rho(\mathbf{r}) - \rho_0$ , and  $\mu_0$  is the chemical potential of the reference liquid. The function  $c^{(2)}$  entering Eq. (6) is the two-body direct correlation function, which is related to the total pair correlation function of the liquid through the Ornstein-Zernike relation. At this level of approximation, the only microscopic information entering the functional is the pair correlation function of the liquid at density  $\rho_0$ .

To study freezing, one writes the density in terms of plane waves as

$$\rho(\mathbf{r}) = \rho_0 (1 + \Delta \rho^*) \left( \sum_{\{\mathbf{G}\}} \hat{\rho}_G e^{i\mathbf{G}\cdot\mathbf{r}} + \text{c.c.} \right), \quad (7)$$

where  $\Delta \rho^*$  is the fractional average density difference between the solid and the liquid phases,  $\{\mathbf{G}\}$  is a sufficient set of nonzero reciprocal lattice vectors, and c.c. is the complex conjugate. The set of Fourier amplitudes  $\hat{\rho}_G$  (or combinations of them) acts as order parameters in this approach, such that the liquid and the crystalline states are defined by  $\hat{\rho}_G = 0$  and  $\hat{\rho}_G \neq 0$ , respectively. At each  $\Delta \rho^*$ ,  $\mathcal{F}$  is then minimized with

respect to all the amplitudes,  $\hat{\rho}_G$ , and phase stability and coexistence regions are obtained using a common tangent construction for the free-energy density as a function of the average density.

Formally, the expansion in Eq. (6) is only valid when the parameter  $\Delta\rho(\mathbf{r})$  is small, which is certainly not true in the solid phase. Nevertheless, it has been shown that even at this level of approximation the classical DFT is capable of describing a liquid-solid phase transition. The agreement of the theory with computer simulations or experiments varies from case to case. For a system of hard spheres, the liquid-fcc transition parameters obtained from the second-order theory are only a few percent off from those obtained from Monte Carlo simulations. In contrast for a classical one-component plasma, the theory is not capable of describing the transition from a liquid to a bcc structure [2].

A connection between the functionals given in Eqs. (1) and (6) can be obtained [3] by first defining the dimensionless density deviation  $n$  as

$$n(\mathbf{r}) = \frac{\rho(\mathbf{r}) - \rho_0}{\rho_0}. \quad (8)$$

Plugging this in Eq. (6) and ignoring the trivial term related to the chemical potential of the liquid, the free-energy change becomes

$$\begin{aligned} \frac{\Delta\mathcal{F}[n(\mathbf{r})]}{k_B T \rho_0} = & \int d\mathbf{r} \{ [1 + n(\mathbf{r})] \ln[1 + n(\mathbf{r})] - n(\mathbf{r}) \} \\ & - \frac{1}{2} \int d\mathbf{r} \int d\mathbf{r}' n(\mathbf{r}) \rho_0 c^{(2)}(|\mathbf{r} - \mathbf{r}'|) n(\mathbf{r}'). \end{aligned} \quad (9)$$

To obtain a functional similar to Eq. (1), two approximations to Eq. (9) are made. First, the local part is expanded as a fourth-order power series as

$$(1 + n) \ln(1 + n) - n \approx \frac{1}{2} n^2 - \frac{a}{6} n^3 + \frac{b}{12} n^4. \quad (10)$$

This expansion differs from the one in Ref. [3] in two respects. First, here both the local and the nonlocal parts of the free energy are expanded around the same reference density. Second, we have included the constants  $a$  and  $b$  in the expansion. The Taylor series expansion made in Ref. [3] is obtained from Eq. (10) by setting  $a=b=1$ . However, as  $n$  is not necessarily a small variable, including the constants  $a$  and  $b$  allows for more freedom in fitting to any desired properties.

Another approximation we make to Eq. (6) is to expand the nonlocal part in terms of gradients. This is most easily done by expanding the direct correlation function in  $k$  space as

$$C(k) \approx C_0 + C_2 k^2 + C_4 k^4, \quad (11)$$

where  $C(k) \equiv \rho_0 \hat{c}(k)$  and  $C_0$ ,  $C_2$ , and  $C_4$  are constants. We note that the same expansion can be obtained also by expanding  $n(\mathbf{r}')$  around  $n(\mathbf{r})$  up to fourth order, revealing the fact that the assumption underlying this approximation is that  $n$  varies slowly compared with the range of  $c^{(2)}$ . The constants  $C_0$ ,  $C_2$ , and  $C_4$  could, in principle, be obtained from an

expansion of  $\hat{c}(k)$ , but in PFC studies so far they have been treated as parameters that are fitted with some other properties of  $\hat{c}(k)$ , e.g., height and position of the main peak [3].

With approximations (10) and (11), the free-energy functional becomes

$$\begin{aligned} \frac{\Delta\mathcal{F}[n(\mathbf{r})]}{k_B T \rho_0} = & \int d\mathbf{r} \left[ n(\mathbf{r}) \frac{1 - C_0 + C_2 \nabla^2 - C_4 \nabla^4}{2} n(\mathbf{r}) - \frac{a}{6} n(\mathbf{r})^3 \right. \\ & \left. + \frac{b}{12} n(\mathbf{r})^4 \right], \end{aligned} \quad (12)$$

which is already mathematically quite similar to Eq. (1). In the Appendix we show how Eq. (1) is exactly recovered from Eq. (12) and how the constants entering these two functionals are related. However, for the remainder of the present paper, we will stick to the notation of Eq. (12) in order to emphasize the connection to the DFT rather than the Swift-Hohenberg equation.

The calculation presented here thus shows that it is possible to derive Eq. (1) from a microscopic DFT. The practical importance of this derivation is that with Eq. (12) it is possible to use the fast numerical methods, including semi-implicit operator splitting [8] and amplitude equations [9] that are not trivially generalized for use with the DFT. However, as the density of the solid phase is extremely inhomogeneous and rapidly varying, the accuracy of Eq. (12) is questionable. Nevertheless, in the following section we address the question as to whether or not the parameters in the PFC model can be chosen to match bulk and surface properties in Fe and compare the results with those of the classical second-order DFT and experiments.

### III. CASE STUDY: IRON

In this section, we show some results of calculations of material properties of iron using functionals given in Eqs. (9) and (12). Iron is a good candidate for this study, because it freezes into a bcc structure, which is the structure that Eq. (12) is known to give rise to. It is also a technically very important material, and preceding attempts to model iron by PFC exist in the literature [4].

#### A. Second-order density-functional theory of freezing

To begin with, we first show the results of calculations performed using Eq. (9). As an input to this DFT calculation, we use a direct correlation function  $\hat{c}(k)$  shown in Fig. 1 derived from the embedded atom method-molecular dynamics (EAM-MD) simulated structure factor from Ref. [4]. This correlation function was simulated at a temperature of  $T = 1772$  K and density of  $\rho_0 = 0.0801 \text{ \AA}^{-3}$ . Since the accuracy of the EAM-MD calculations is questionable in the small  $k$  limit, the  $k=0$  mode of  $\hat{c}(k)$  was fit to the theoretical prediction of Tsu and Takano [10] for the isothermal compressibility of iron at  $T = 1833$  K, which is  $\kappa_T = 1.04 \times 10^{-11} \text{ m}^2 \text{ N}^{-1}$ . Using these values, together with Jimbo and Cramb's [11] experimental expression for the density of liquid iron at  $T = 1833$  K, we obtain the estimate  $\rho_0 \hat{c}(0) = 1 - (\kappa_T \rho_0 k_B T)^{-1} \approx -49$ , which will be used in this work.

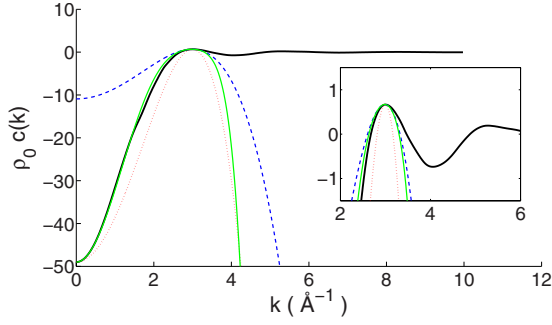


FIG. 1. (Color online) Full  $\hat{c}(k)$  used in our DFT calculations (black solid line) and the expansions used in our different PFC models: green solid line is the eighth-order fit (EOF), blue dashed line is the GL fit, and red dotted line is the three parameter fit to  $C_0$  and the first maximum.

To calculate the bulk thermodynamic properties of solid iron from Eq. (9), we have employed a simple Picard iteration procedure. One unit cell with periodic boundary conditions is used in these calculations. The initial configuration is a sum of discrete delta functions at the lattice sites in the unit cell. Based on the density profile at the  $i$ th iteration, we generate the one-body direct correlation function  $c^{(1)}(\mathbf{r};[n])$ , which we use to calculate the  $(i+1)$ th density profile according to  $\ln(1+n) \propto c^{(1)}$ , such that the average density of the system is conserved in each iteration step. For a given average density and lattice spacing, a few hundred iterations are required for convergent results. At each average density, the calculation is repeated with several sizes of the unit cell to minimize the free-energy density with respect to the lattice spacing. Thus, our calculation does not impose any restriction on the vacancy concentration of the system.

The results of the free-energy density calculations for liquid and bcc phases are shown in Fig. 2 and example plots of (100) faces of density profiles of bcc and fcc phases are shown in Fig. 3. Coexistence densities are obtained from the free-energy densities by the standard common tangent construction. Most importantly, we find a transition from liquid to bcc at  $\rho_l/\rho_0=1.097$  and  $\rho_{bcc}/\rho_0=1.126$ , giving a coexistence gap  $(\rho_{bcc}-\rho_l)/\rho_l=2.7\%$  that is consistent with experi-

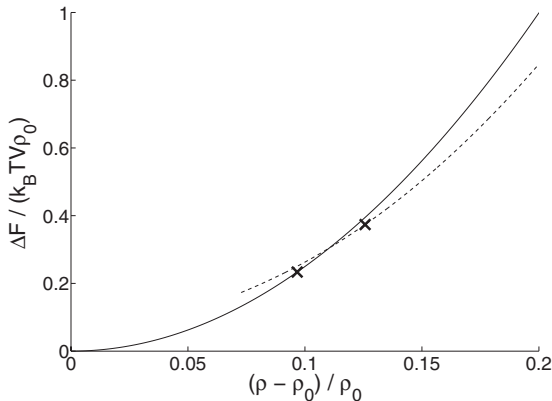


FIG. 2. Free energies of liquid (solid line) and bcc (dashed line) phases in second-order DFT. Crosses show the coexistence points obtained by double tangent construction.

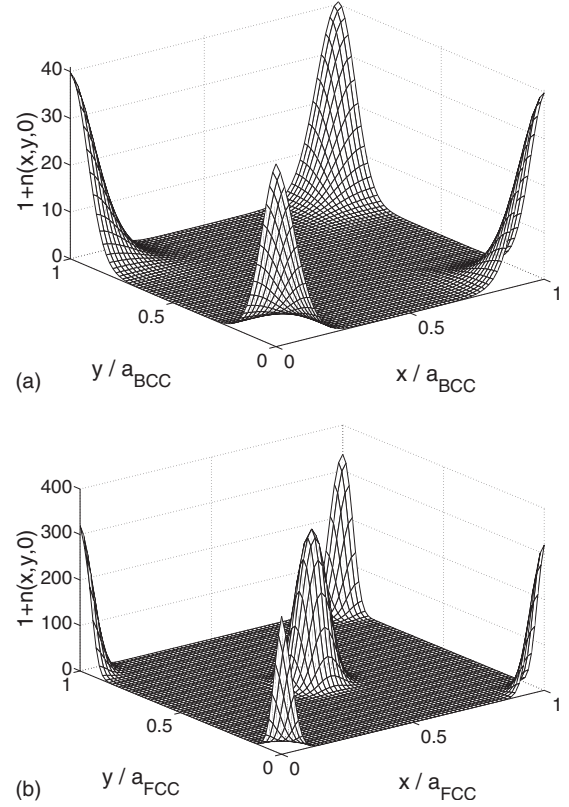


FIG. 3. Local densities in (100) crystal planes of bcc coexisting with liquid (above) and fcc coexisting with bcc (below) from DFT.

ment. More specifically this gap gives a volume change on melting of  $\Delta V=0.29 \text{ \AA}^3$  per atom in reasonable agreement with the experimental value of  $\Delta V=0.38 \text{ \AA}^3$  per atom [12]. The lattice spacing of the bcc coexisting with the liquid turns out to be  $a_{bcc}=2.95 \text{ \AA}$ . However, this lattice spacing corresponds to a *negative* vacancy concentration, which we estimate to be  $c_V \approx -16\%$  (i.e.,  $\approx 2.32$  atoms per unit cell). This results from the fact that as there is no constraint to the number of atoms per lattice sites, the minimum free-energy distance between lattice sites is defined by the positions of the peaks in  $\hat{c}(k)$ , and not by the average density. In DFT studies, this problem is usually avoided by varying the reference density, and thus the positions of the peaks, along with the average density of the solid [2]. Of course, if the DFT were an accurate approximation of the underlying system, it would be able to predict the vacancy concentration without additional adjustments, as in the case of hard spheres in the fundamental measure DFT [13]. However, that is not the case for the current approximation.

The bulk modulus of the different phases can be calculated from the free-energy curves according to the thermodynamic relation

$$B_T = \rho^2 \left( \frac{\partial^2 (F/V)}{\partial \rho^2} \right)_T. \quad (13)$$

The results are  $B_T^l=98.0 \text{ GPa}$  for the liquid at  $\rho=\rho_0$ , and  $B_T^{bcc}=101.7 \text{ GPa}$  for the bcc at coexistence with the liquid. We note that these values were obtained by imposing no

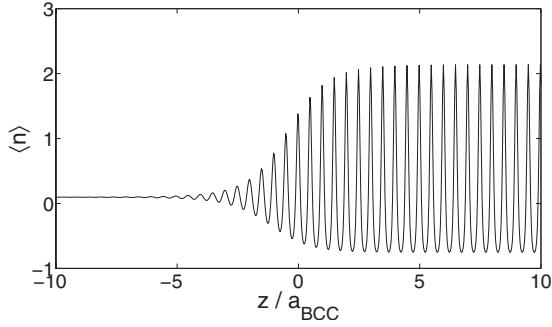


FIG. 4. Density profile of (110) bcc-liquid interface in second-order DFT.  $z$  here is the axis perpendicular to the surface, measured in equilibrium lattice spacings of the bcc phase, and  $\langle n \rangle = A^{-1} \int \int n(x, y, z) dx dy$ .

constraint on the relation between lattice spacing and average density.

To our knowledge, the bulk modulus of bcc iron has been measured experimentally only up to about  $T=820$  °C, where it reaches a value of  $B_T^{bcc} = 135$  GPa [14]. On the other hand, from the room temperature up to  $T=820$  °C there is a monotonically decreasing trend in  $B_T^{bcc}$  vs  $T$  [14]. If we assume that this trend is linear up to the melting temperature, we get an estimate  $B_T^{bcc} \approx 105$  GPa at  $T=1772$  K in very good agreement with our DFT result.

When further increasing the density, this theory is also able to describe a transition from bcc to fcc structure, taking place at  $\rho_{bcc}/\rho_0 = 1.772$  and  $\rho_{fcc}/\rho_0 = 1.789$ . At such high density, it comes as no surprise that the physical properties of the fcc phase given by this density expansion do not agree very well with experimental data.

In addition to bulk thermodynamic properties, we have also calculated the bcc-liquid surface density profile and free energies on (100) and (110) crystal planes. For these calculations, we use a quasi-one-dimensional slab, whose size is one unit cell in the directions perpendicular to the surface and 128 unit cells parallel to the surface. Half of the system is then initialized as solid, and half of it as liquid. The surface density profile is found using the same Picard iteration procedure as for the bulk properties, with the exception that mixing between successive iterations is now required to stabilize the calculation. Surface free energies are then calculated by subtracting the bulk contribution from the total free energy of the system containing the interface. Surface energies turn out to be  $\sigma_{100} = 89.20$  ergs/cm<sup>2</sup>,  $\sigma_{110} = 91.93$  ergs/cm<sup>2</sup>, and  $\sigma_{111} = 86.9$  ergs/cm<sup>2</sup>, giving an anisotropy coefficient  $\epsilon_4 = (\sigma_{100} - \sigma_{110}) / (\sigma_{100} + \sigma_{110}) = 1.5\%$ . A plot of the  $(x, y)$  averaged density of (110) surface is shown in Fig. 4. The surface free energies disagree with the results of MD simulations by about a factor of 2. To be more precise, the MD gives  $\sigma_{100} = 177.0$  ergs/cm<sup>2</sup>,  $\sigma_{110} = 173.5$ , and  $\epsilon_4 = 1.0\%$ , using the same potential that was used for obtaining  $\hat{c}(k)$  used in the present work [4].

### B. Phase-field-crystal model

After calculating the main physical properties of iron using the full second-order DFT, we now turn our attention to

the PFC model to see how well it is able to capture the properties of DFT. Before presenting the results of our PFC calculations, we point out that it should be obvious that the density deviation field  $n$  is neither small nor slowly varying in space. Therefore approximations (10) and (11) may not be good approximations to the classical DFT results.

We used a Taylor series expansion, i.e., setting  $a=b=1$  in Eq. (10) and fitting the three coefficients in Eq. (11) to  $k=0$  limit, and height and position of the first peak in  $\hat{c}(k)$ , in the spirit suggested in [3]. For our calculations, we have used both the analytical one-mode approximation

$$n(\mathbf{r}) = n_0 + (1 + n_0)4u[\cos(qx)\cos(qy) + \cos(qx)\cos(qz) + \cos(qy)\cos(qz)], \quad (14)$$

and a numerical annealing based on Eq. (2). In Eq. (14),  $n_0$  is the average density and  $u$  is the density wave amplitude corresponding to the principal set of the reciprocal lattice vectors. With this fitting procedure we found the solid phase to be unstable at all average densities. The reason for this is the fact that, as we already pointed out, approximations (10) and (11) are not consistent with the original DFT.

Calculations were performed to separately examine the validity of the two approximations used, i.e., Eqs. (10) and (11). We found that replacing the gradient expansion with the full nonlocal term is not sufficient to stabilize the solid. On the other hand, if we expand  $\hat{c}(k)$ , but leaving the logarithmic term unexpanded, we do find that there exists a stable bcc solution. The problem is that the bcc only stabilizes at a much higher density than in the DFT, and the free-energy difference between solid and liquid is very much smaller than in the DFT. The coexistence densities are  $\rho_l/\rho_0 = 1.358$  and  $\rho_{bcc}/\rho_0 = 1.361$ , giving a coexistence gap of only  $(\rho_{bcc} - \rho_l)/\rho_l \approx 0.2\%$ . In this approximation the density profile of the bcc phase is very much like the one-mode approximation and significantly different from the DFT result shown in Fig. 3. Finally, we found that if  $n$  is expanded around the average density  $\bar{\rho}$  instead of  $\rho_0$ , as in the original derivation [3] of the PFC from the classical DFT, then a stable one-mode-like bcc structure appears at  $\rho_{bcc}/\rho_0 \approx 1.409$ . The coexistence gap obtained by the double tangent construction is even smaller than 0.1% in this case, with the exact coexistence densities in a given simulation slightly depending on  $\bar{\rho}$  chosen.

These results indicate that deriving PFC parameters from the second-order DFT (which itself predicts some unphysical behavior) as presented in Ref. [3] leads to very inaccurate results. This naturally leads to the question, is it possible to fit the parameters of the PFC free energy [i.e., either Eq. (1) or Eq. (12)] in such a manner that reasonable predictions can be made? To examine this possibility we consider the approach taken by WK who proposed such a method for the case of iron [4]. In their method they used the height, the position, and the second derivative of the first peak in  $C(k) \equiv \rho_0 \hat{c}(k)$  to fit the linear parts of the free energy. The nonlinear coefficients are fitted such that for average density  $\rho_0$  the free energy of the solid phase equals that of the liquid phase, with a correct amplitude of density fluctuations obtained from a molecular dynamics (MD) simulation.

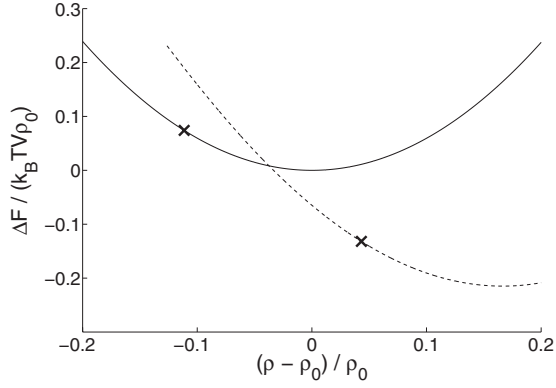


FIG. 5. Free energies of liquid (solid line) and bcc (dashed line) phases in the GL PFC model. Crosses show coexistence points obtained by the double tangent construction.

We will now adapt a scheme for obtaining the parameters for the free energy used in the present work. This scheme is a simplified version of the small- $\epsilon$  analysis based scheme in Ref. [4] and since it is inspired by the Ginzburg-Landau theory [15], we call this fitting method the GL PFC model. First, for the linear part we fit the parameters in Eq. (11) to reproduce the numbers given in Ref. [4],  $1/S(k_m)=1-C(k_m)=0.332$ ,  $C''(k_m)=-10.40 \text{ \AA}^2$ , and  $k_m=2.985 \text{ \AA}^{-1}$ , which is the position of the first maximum. The parameters turn out to be  $C_0=-10.9153$ ,  $C_2=2.6 \text{ \AA}^2$ , and  $C_4=-0.1459 \text{ \AA}^4$ . We then use the one-mode approximation [Eq. (14)] to find how to choose the nonlinear coefficients  $a$  and  $b$ , such that the amplitude  $u$  in Eq. (14) that minimizes the free energy is  $u_s=0.72$ , as defined from a MD simulation [4], and that the free energies of liquid and bcc phases at that minima are equal. The resulting relations are

$$a = \frac{3}{2S(k_m)u_s}, \quad b = \frac{4}{30S(k_m)u_s^2}, \quad (15)$$

which with the present numbers give  $a=0.6917$  and  $b=0.08540$ , which are notably far from unity, i.e., the values obtained by expanding the second-order DFT [3].

The results of the numerical calculations for the free energy are shown in Fig. 5. There is a stable body-centered-cubic solid phase, with coexistence densities  $\rho_l/\rho_0=0.889$  and  $\rho_{bcc}/\rho_0=1.043$ . Again, the density profile of the bcc

phase looks similar to the one-mode approximation in contrast to the DFT result with unphysical negative densities in between the maxima. The volume difference between the bcc and the liquid phases is  $\Delta V=2.07 \text{ \AA}^3$  per atom, which is significantly larger than the experimental value of 0.38. This is most likely due to the fact that in this fitting procedure the absolute value of  $k=0$  value of  $\rho_0\hat{c}(k)$  (i.e.,  $|C_0|$ ) is five times smaller than the experimental value, implying a significantly larger isothermal compressibility of the liquid state. The bulk moduli of the phases at coexistence, as calculated from the free-energy curves, are indeed quite small:  $B_T^l=18.6 \text{ GPa}$  and  $B_T^{bcc}=22.2 \text{ GPa}$ . An explanation to why the smaller bulk moduli impose a larger coexistence gap can be obtained by expanding the free energies of liquid and bcc phases to the second order in density around the point where liquid coexists with bcc. By making certain approximations, we see that the coexistence gap scales roughly as the inverse of  $B_T$ , in an agreement with a comparison of the current fitting method with experiments ( $\Delta V_{\text{expt}}/\Delta V_{\text{GL}} \approx B_{\text{GL}}^l/B_{\text{expt}}^l$ ). The procedure does, however, predict surface free energies that are in reasonable agreement with MD, as shown earlier by Wu and Karma [4]. These are  $\sigma_{100}=207.11 \text{ ergs/cm}^2$  and  $\sigma_{110}=201.67 \text{ ergs/cm}^2$ , giving  $\epsilon_4=(\sigma_{100}-\sigma_{110})/(\sigma_{100}+\sigma_{110})=1.3\%$  compared with the MD simulation results in Table I.

We note that two approximations are employed when choosing the nonlinear parameters by Eqs. (15). First, the one-mode approximation was used instead of the full numerical minimization, resulting in slightly inaccurate density wave amplitudes and free energies. Second, the condition of equal free energies at  $\rho=\rho_0$  only holds at the limit of weakly first-order transition. More generally, the proper conditions are (i) the free energy of the liquid at  $\rho=\rho_0$  has a common tangent with free energy of the solid at a higher density  $\rho_{bcc}$  and (ii) the amplitude of the first mode of density fluctuations of the solid phase at  $\rho=\rho_{bcc}$  is  $u_s$ . In an attempt to improve this fitting method, we have also fitted the nonlinear coefficients numerically, without making the previously described approximations. The resulting coefficients are  $a=0.5687$  and  $b=0.0660$ . With this parameter set, the physical properties we investigated are  $\rho_l/\rho_0=1.000$  (as fitted),  $\rho_{bcc}/\rho_0=1.134$ ,  $B_T^l=23.3 \text{ GPa}$ , and  $B_T^{bcc}=26.3 \text{ GPa}$  while  $\sigma_{100}=196.40 \text{ ergs/cm}^2$ ,  $\sigma_{110}=196.41$ , and  $\sigma_{111}=184.85$ . Thus, the conclusion about the fitting method remains unaltered: surface free energies are quantitatively well captured, but bulk free energies as a function of the average density are not.

TABLE I. Comparison of physical quantities of iron in different models with experiments and molecular dynamics simulations.

Quantity	Expt./MD	DFT	GL PFC	EOF PFC
Expansion in melting ( $\text{\AA}^3/\text{atom}$ )	<b>0.38</b> [12]	0.29	2.07	0.43
Solid bulk modulus (GPa)	<b>105</b> [14] <sup>a</sup>	101.7	22.2	94.5
Liquid bulk modulus (GPa)	<b>96.2</b> [10]	98.0	18.6	93.2
Surface energy (100) (ergs/cm <sup>2</sup> )	177.0 [4]	91.9	207.1	165.7
Surface energy (110) (ergs/cm <sup>2</sup> )	173.5 [4]	89.2	201.7	161.5
Surface energy (111) (ergs/cm <sup>2</sup> )	173.4 [4]	86.9	194.8	157.2
Anisotropy $\epsilon_4$ (%)	1.0 [4]	1.5	1.3	1.3

<sup>a</sup>Linear extrapolation from lower temperatures.

### C. Eighth-order fitting method for the phase-field-crystal model

The results of the preceding section indicate that it is quite difficult to simultaneously obtain accurate results for the surface energies, miscibility gap, isothermal compressibility of the liquid state, and the bulk modulus using the PFC-type free-energy functional given in Eq. (12). The analysis of WK [4,15] indicates that the factors defining the surface free energy in the PFC model are  $u_s$ ,  $k_m$ ,  $S(k_m)$ , and  $C''(k_m)$ . On the other hand,  $C_0$  is an important quantity in defining the bulk moduli of the phases and the size of the coexistence gap. To improve the PFC model, we would like to include all the four quantities  $C_0$ ,  $k_m$ ,  $S(k_m)$ , and  $C''(k_m)$  in the correlation function of this model. Unfortunately, there are only three parameters in Eq. (11), making it impossible to fit in all the four quantities. For this reason, we propose a method of expanding the correlation function

$$\rho_0 \hat{c}(k) \approx C(k_m) - \Gamma \left( \frac{k_m^2 - k^2}{k_m^2} \right)^2 - E_B \left( \frac{k_m^2 - k^2}{k_m^2} \right)^4. \quad (16)$$

We call this expansion the eighth-order fitting (EOF) method, because the expansion includes gradients up to the eighth order. Using EOF, it is possible to fit all the important properties mentioned earlier, by choosing the parameters as

$$\Gamma = -\frac{k_m^2 C''(k_m)}{8}, \quad (17)$$

$$E_B = C(k_m) - C_0 - \Gamma. \quad (18)$$

By plugging in the parameters of WK and  $C_0 = -49$ , we get  $\Gamma = 11.583$  and  $E_B = 38.085$ . As can be seen from Fig. 1, this polynomial fits the  $\hat{c}(k)$  curve up to the first peak much better than the previously described fourth-order polynomials. The nonlinear parameters  $a$  and  $b$  are obtained by the one-mode approximation in order to avoid the unnecessary complication of the numerical fitting procedure. For  $n_0 = 0$  a one-mode approximation to the expansion gives exactly the same result as in the fourth-order expansion. Thus, the nonlinear coefficients are again given by Eqs. (15).

The free-energy curves of different phases in the EOF model are shown in Fig. 6. The coexistence between the liquid and the bcc crystal structure is located at  $\rho_l/\rho_0 = 0.975$  and  $\rho_{bcc}/\rho_0 = 1.009$ , giving a very reasonable  $(\rho_{bcc} - \rho_l)/\rho_l = 3.4\%$  for the coexistence gap. Although the coexistence gap is still slightly larger than in the DFT, we consider this result as a significant improvement over the previous methods, which overestimate the coexistence gap by almost an order of magnitude. In fact, the volume change in melting is fortuitously even closer to the experimental value than in the DFT, being  $\Delta V = 0.43 \text{ \AA}^3$  per atom (experiment:  $\Delta V = 0.38 \text{ \AA}^3$  per atom [12]; DFT:  $\Delta V = 0.29 \text{ \AA}^3$  per atom). The density field of the bcc phase looks again very much like the one-mode approximation, as can be seen from Fig. 7. Examining the density profile in more detail, we find that the amplitudes of the Fourier modes go rapidly to zero as  $k$  increases. For example, the amplitude corresponding to the second star of the reciprocal lattice vectors is only about 1% of the amplitude of the first set of modes.

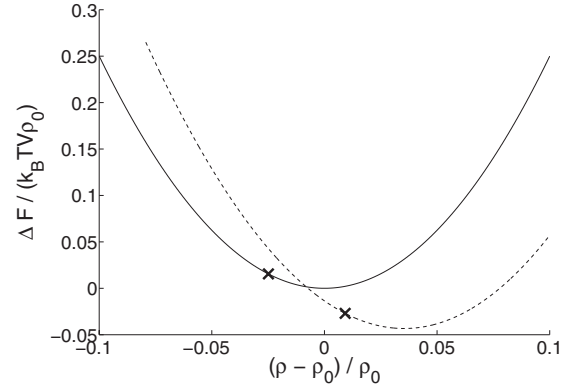


FIG. 6. Free energies of liquid (solid line) and bcc (dashed line) phases in the EOF PFC model. Crosses show coexistence points obtained by double tangent construction.

The bulk moduli of liquid and bcc phases at coexistence, as calculated from the free-energy curves, are also an improvement to the previous method,  $B_T^l = 93.2 \text{ GPa}$  and  $B_T^{bcc} = 94.5 \text{ GPa}$ . The surface free energies are  $\sigma_{100} = 165.66 \text{ ergs/cm}^2$ ,  $\sigma_{110} = 161.50 \text{ ergs/cm}^2$ , and  $\sigma_{111} = 157.16 \text{ ergs/cm}^2$ . These numbers are in better agreement with simulations than the ones obtained from the previous fitting scheme, and the anisotropy coefficient  $\epsilon_4$  turns out to have the same value of  $\epsilon_4 = 1.3\%$ . The fact that the surface free energies are improved over the previous method is probably related to the fact that the difference between the aver-

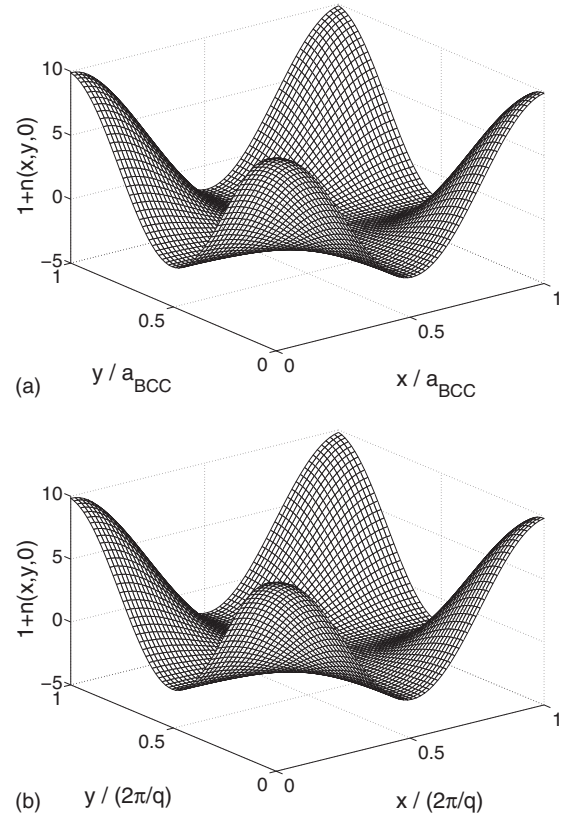


FIG. 7. Local density  $n$  in (100) crystal planes of bcc coexisting with liquid (above) in the EOF PFC model. Below is the one-mode approximation with  $n_0 = 0.009$  and  $u = 0.734$  for comparison.

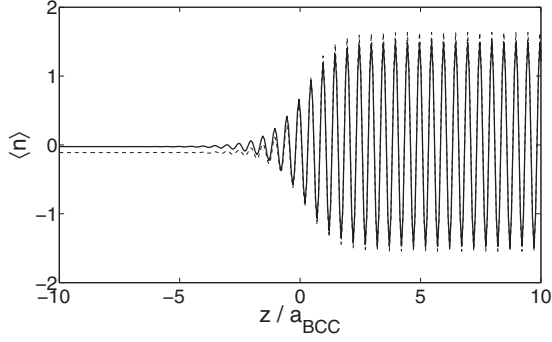


FIG. 8. Profiles of (110) bcc-liquid surface in PFC models. Solid line is obtained from the present EOF PFC functional, and dashed line is from the GL fitting method.  $z$  and  $\langle n \rangle$  are defined as in Fig. 4.

age densities of the two phases is smaller. The profile of the (110) bcc-liquid surface in EOF is illustrated in Fig. 8 with comparison to the GL fitting method. The two are in good agreement.

Overall, the results obtained by the EOF are very encouraging, even though the density is still unphysically widespread around the lattice sites and can even be negative in between them. The field  $n$  should probably be interpreted as a locally averaged, or weighted density difference, where the higher-order Fourier modes are washed out by the weighting procedure. If the model is interpreted in this way, it is a promising choice for bcc materials, because the numerical advantages to the DFT model are significant. We may also argue that, in the uniform limit, both the PFC dynamical equation (2) with the present functional, and the dynamical DFT equation of Marconi and Tarazona [16] linearize to

$$\frac{\partial \hat{n}(k)}{\partial t} = -k^2 [1 - \rho_0 \hat{c}(k)] \hat{n}(k). \quad (19)$$

Because the function  $\hat{c}(k)$  is approximately the same in the two models up to the first peak, the dynamics of the longer wavelengths should be no different in the two models, although the shorter wavelengths vanish faster in the PFC model. On the other hand, in the uniform solid the two models can be made to reach equilibrium with the same value of  $\hat{n}(k_m)$ .

Finally, we note that although here we used MD simulation data as an input for the EOF-PFC model, this might not be necessary if one wishes to generalize this model to other bcc materials. All that is needed from the correlation function is the  $k=0$  limit, the maximum value  $C(k_m)$ , the position of the maximum value  $k_m$ , and the second derivative at the peak  $C''(k_m)$ . The  $k=0$  limit is related to the compressibility of the liquid through the compressibility equation; for  $C(k_m)$  we have the Hansen-Verlet freezing criterion, which states that simple liquids freeze when  $S(k_m)$  reaches  $2.9 \pm 0.1$  [2,7,17]; and  $k_m$  is simply related to the lattice spacing of the solid. If these three were known, the only thing we would need is  $C''(k_m)$ , which could also be fitted with an experimental value for the surface free energy. For the nonlinear coefficients we also need the first mode amplitude  $u_s$ , for

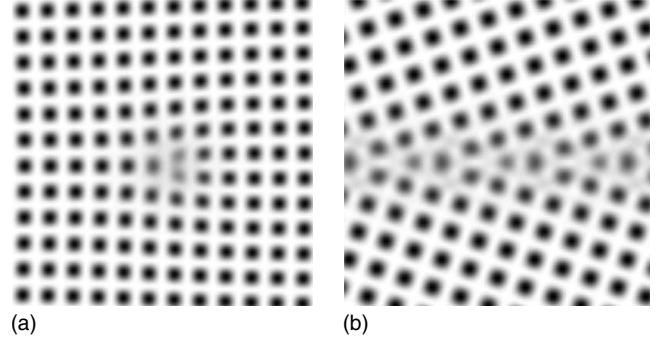


FIG. 9. Sample grain boundaries for misorientation angles of  $1.79^\circ$  and  $36.86^\circ$  for the above and below configurations, respectively. In these figures the grayscale corresponds to  $n(x, y, 0)$ , with the  $z$  axis parallel to the grain boundary.

which it is possible to obtain an estimate from the Lindemann melting criterion [2]. Thus, if we consider the values of  $u_s$  and  $S(k_m)$  to be universal, this would fix all the nonlinear and one of the linear coefficients of the model. After that and scaling out the length scale  $k_m$ , we would be left with a model that should give a well description of many material properties with only two parameters  $E_B$  and  $\Gamma$ .

#### D. Grain boundary energy in Fe

The free-energy functional and parameters presented in the preceding section now provide a model of Fe that gives a very good approximation to the surface tension, its anisotropy, the liquid state compressibility, the bulk modulus, and the miscibility gap. The model can now be exploited to make predictions for other quantities such as the grain boundary energy. Numerical simulations were conducted to measure the energy ( $\gamma$ ) per unit area of a [001] symmetric tilt grain boundary as a function of grain misorientation angle ( $\theta$ ). The calculations were performed at a density of  $(\rho - \rho_0)/\rho_0 = 0.030$ , which is just above the density of the solid at coexistence. Sample configurations are shown in Fig. 9 for both low and high angle boundaries. The free energy per unit area of the boundaries is shown as a function  $\theta$  in Fig. 10.

As can be seen in Fig. 10 the grain boundary energy increases with increasing mismatch angle, mainly due to a corresponding increase in the density of dislocations. For small angles Read and Shockley [18] derived the following expression for the grain boundary energy:

$$\gamma = \frac{Ga}{4\pi(1-\sigma)} [A - \ln(\theta)], \quad (20)$$

where  $G$  is the rigidity modulus,  $a$  is the lattice constant,  $\sigma$  is Poisson's ratio, and  $A$  is a complex factor that Read and Shockley estimated to be 0.45. In two dimensions the parameter  $A$  can be obtained by assuming that the dislocation core size is chosen to minimize  $\gamma$ . This gives  $A = 3/2 - \ln(2\pi) \approx -0.34$ , which agrees very well with numerical calculations [1]. The inset in Fig. 10 shows a fit of the numerically obtained data with the Read-Shockley equation for small angles. The best fit gives  $G = 31.7$  GPa and  $A = -0.41$ , assuming  $\sigma = 1/3$ . Independently from the grain boundary

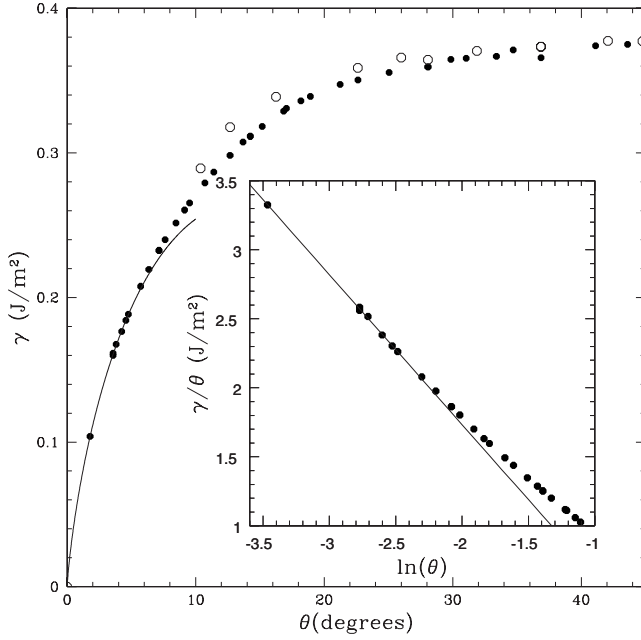


FIG. 10. Grain boundary energy  $\gamma$  for Fe as a function of misorientation angle. The solid points correspond to mismatch angles of  $0^\circ$ – $45^\circ$ , while the open points correspond to  $90^\circ$ – $\theta$  for angles between  $45^\circ$  and  $90^\circ$ . In the inset,  $\gamma/\theta$  is plotted against  $\ln(\theta)$ , where in this instance  $\theta$  is in radians. The solid line is a best fit to a straight line given by  $\gamma/\theta = -[0.44089 + 1.087 \ln(\theta)] \text{ J/m}^2$

calculations, we have also performed numerical shearing experiments with our PFC model, from which we estimate the shear modulus to be  $G \approx 53 \text{ GPa}$ , in moderate agreement with the fitted value.

Experimentally, the grain boundary energy of  $\delta$  iron has been determined to be  $468 \text{ mJ/m}^2$  [19]. As real materials contain more large-angle grain boundaries than small-angle ones, it is most reasonable to compare the experimental value with the large-angle grain boundary energies obtained from our model. Therefore, the experimental value agrees reasonably well with our result, where the maximum grain boundary energy is approximately  $380 \text{ mJ/m}^2$ . Interestingly, according to [19] the solid-liquid surface free energy of iron is  $204 \text{ mJ/m}^2$ , so the ratio between solid-liquid and grain boundary energies  $\sigma_{GB}/\sigma_{s-l} \approx 2.29$  agrees well with the present result  $\sigma_{GB}/\sigma_{s-l} \approx 2.16$ .

The only previous study of the angular dependence of grain boundary energy in iron, at least to our knowledge, has been conducted using a modified analytical embedded atom method by Zhang *et al.* [20] at zero temperature. In this limit the data are an order of magnitude greater than reported here and inconsistent with the Read-Shockley (RS) equation.

#### IV. CONCLUSIONS

We have studied free-energy functionals used in phase-field-crystal (PFC) models and compared them with the second-order density-functional theory (DFT) of freezing, by using iron as an example case. The comparison of PFC and DFT revealed quite significant differences between these two

theories. Most importantly, the derivation of PFC from the DFT cannot be considered a reliable way of obtaining the parameters for PFC. By fitting the parameters in a more *ad hoc* way, our results confirm the argument of Wu and Karma that by fitting in the correct height and second derivative of the first peak in the direct correlation function, and the correct amplitude of density fluctuations in the solid corresponding to the principal set of reciprocal lattice vectors, one obtains a very reasonable estimate for the surface free energy of the material. However, as our results show that bulk moduli of the phases and coexistence gap between solid and liquid phases turn out to be less accurate. To fix this problem, we have presented a way of expanding the correlation function up to eighth order. Our results show that this EOF method solves the problems with bulk moduli and coexistence gap. We have also applied the EOF-PFC model to calculating grain boundary energies of iron near its melting point. We consider the EOF as a likely candidate for being used in future PFC studies, at least if any quantitative accuracy of the results is desired.

#### ACKNOWLEDGMENTS

This work was supported in part by the Academy of Finland through its Center of Excellence COMP grant, Tekes through its MASIT33 project, and EU Grant No. STRP 016447 MagDot. A.J. acknowledges financial support from the Finnish Academy of Science and Letters. K.R.E. acknowledges support from NSF under Grant No. DMR-0413062. We also wish to thank CSC-Scientific Computing Ltd. for computational resources.

#### APPENDIX: DERIVATION OF THE SWIFT-HOHENBERG FREE ENERGY FROM THE DFT

In Sec. II we show how a functional that resembles the Swift-Hohenberg free energy [Eq. (1)] is obtained from the classical density-functional theory. Here, we show how Eq. (1) is exactly recovered from Eq. (12) and how the constants entering these functionals are related. We begin by rewriting Eq. (12) as

$$\frac{\Delta\mathcal{F}[n(\mathbf{r})]}{k_B T \rho_0} = \int d\mathbf{r} \left\{ \frac{n(\mathbf{r})}{2} \left[ \frac{1}{S(k_m)} + \frac{\Gamma}{k_m^4} (k_m^2 + \nabla^2)^2 \right] n(\mathbf{r}) - \frac{a}{6} n(\mathbf{r})^3 + \frac{b}{12} n(\mathbf{r})^4 \right\}, \quad (\text{A1})$$

where  $k_m$  is position of the first peak in  $C(k)$  [or  $S(k)$ ] and  $S(k_m)$  is the peak value of the structure factor.  $\Gamma$  is given by Eq. (17) for the GL-PFC model, or  $\Gamma = C(k_m) - C(0)$  for the Taylor series expansion. We then rewrite the field  $n$  as

$$n(\mathbf{r}) = \bar{n} + \frac{\phi(\mathbf{r})}{\rho_0}, \quad (\text{A2})$$

where  $\bar{n}$  is a constant and  $\phi(\mathbf{r})$  is an order-parameter field with the unit of the number density. By plugging this in Eq. (A1), defining  $F$  as the difference in free energy from  $\mathcal{F}[\bar{n}]$

and ignoring terms that are constant or linearly proportional to  $\phi$ , we get

$$F[\phi(\mathbf{r})] = \int d\mathbf{r} \left\{ \frac{\phi(\mathbf{r})}{2} \left[ \frac{k_B T}{\rho_0} [S(k_m)^{-1} - a\bar{n} + b\bar{n}^2] + \frac{k_B T \Gamma}{\rho_0 k_m^4} (k_m^2 + \nabla^2)^2 \right] \phi(\mathbf{r}) - \frac{k_B T}{\rho_0^2} \left( \frac{a}{6} - \frac{\bar{n}b}{3} \right) \phi(\mathbf{r})^3 + \frac{1}{4} \frac{k_B T b}{3\rho_0^3} \phi(\mathbf{r})^4 \right\}. \quad (\text{A3})$$

From here, we see that the cubic term can be made to vanish by choosing

$$\bar{n} = \frac{a}{2b}. \quad (\text{A4})$$

After making this substitution, Eq. (A3) becomes

$$F[\phi(\mathbf{r})] = \int d\mathbf{r} \left\{ \frac{\phi(\mathbf{r})}{2} \left[ \frac{k_B T}{\rho_0} \left( \frac{1}{S(k_m)} - \frac{a^2}{4b} \right) + \frac{k_B T \Gamma}{\rho_0 k_m^4} (k_m^2 + \nabla^2)^2 \right] \phi(\mathbf{r}) + \frac{1}{4} \frac{k_B T b}{3\rho_0^3} \phi(\mathbf{r})^4 \right\}. \quad (\text{A5})$$

This equation is mathematically exactly of the same form as Eq. (1), and the parameters can now be identified as

$$q_0 = k_m, \quad (\text{A6})$$

$$\alpha = \frac{k_B T}{\rho_0} \left( \frac{1}{S(k_m)} - \frac{a^2}{4b} \right), \quad (\text{A7})$$

$$\lambda = \frac{k_B T \Gamma}{\rho_0 k_m^4}, \quad (\text{A8})$$

$$g = \frac{k_B T b}{3\rho_0^3}. \quad (\text{A9})$$

In order to compare the present work with the work of Wu and Karma [4], it is interesting to note that in our GL fit, where  $a$  and  $b$  are given by Eqs. (15) and  $\Gamma$  is given by Eq. (17), we get for the linear parameters

$$\alpha = \frac{-103k_B T}{32\rho_0 S(k_m)}, \quad (\text{A10})$$

$$\lambda = -\frac{k_B T C''(k_m)}{8\rho_0 k_m^4}, \quad (\text{A11})$$

which are exactly the same results as given by Eqs. (41) and (42) of Ref. [4]. For the nonlinear coefficient  $g$  we get

$$g = \frac{2k_B T}{45\rho_0^3 u_s^2 S(k_m)}, \quad (\text{A12})$$

which is also the same as given by Wu and Karma, after a minor error in Eq. (45) of Ref. [4] is corrected. Thus, our GL fit results in the same Swift-Hohenberg equation as the small- $\epsilon$  analysis of Wu and Karma, even though the procedures for obtaining the parameters are different.

- 
- [1] K. R. Elder, M. Katakowski, M. Haataja, and M. Grant, *Phys. Rev. Lett.* **88**, 245701 (2002); K. R. Elder and M. Grant, *Phys. Rev. E* **70**, 051605 (2004).
- [2] Y. Singh, *Phys. Rep.* **207**, 351 (1991).
- [3] K. R. Elder, N. Provatas, J. Berry, P. Stefanovic, and M. Grant, *Phys. Rev. B* **75**, 064107 (2007).
- [4] (a) K.-A. Wu and A. Karma, *Phys. Rev. B* **76**, 184107 (2007); (b) K.-A. Wu, Ph.D. thesis, Northeastern University, 2006.
- [5] J. Swift and P. C. Hohenberg, *Phys. Rev. A* **15**, 319 (1977).
- [6] T. V. Ramakrishnan and M. Yussouff, *Phys. Rev. B* **19**, 2775 (1979).
- [7] J.-P. Hansen and I. R. McDonald, *Theory of Simple Liquids*, 3rd ed. (Academic, Amsterdam, 2006).
- [8] G. Tegze, G. Bansal, G. I. Tóthb, T. Pusztai, Z. Fan, and L. Gránásy, *J. Comput. Phys.* **228**, 1612 (2009); B. P. Vollmayr-Lee and Andrew D. Rutenberg, *Phys. Rev. E* **68**, 066703 (2003); J. Zhu, L.-Q. Chen, J. Shen, and V. Tikare, *ibid.* **60**, 3564 (1999).
- [9] B. P. Athreya, N. Goldenfeld, and J. A. Dantzig, *Phys. Rev. E* **74**, 011601 (2006).
- [10] Y. Tsu and K. Takano, *88th Spring Conference* (Japan Institute of Metals, Sendai, 1981), Vol. 88, p. 86; T. Itami and M. Shimoji, *J. Phys F: Met. Phys.* **14**, L15 (1984).
- [11] I. Jimbo and A. W. Cramb, *Metall. Mater. Trans. B* **24**, 5 (1993).
- [12] M. I. Mendeleev, S. Han, D. J. Srolovitz, G. J. Ackland, D. Y. Sun, and M. Asta, *Philos. Mag.* **83**, 3977 (2003).
- [13] Y. Rosenfeld, M. Schmidt, H. Löwen, and P. Tarazona, *J. Phys.: Condens. Matter* **8**, L577 (1996).
- [14] D. J. Dever, *J. Appl. Phys.* **43**, 3293 (1972); J. J. Adams, D. S. Agosta, R. G. Leisure, and H. Ledbetter, *ibid.* **100**, 113530 (2006).
- [15] K.-A. Wu, A. Karma, J. J. Hoyt, and M. Asta, *Phys. Rev. B* **73**, 094101 (2006).
- [16] U. M. B. Marconi and P. Tarazona, *J. Phys.: Condens. Matter* **12**, A413 (2000).
- [17] J.-P. Hansen and L. Verlet, *Phys. Rev.* **184**, 151 (1969).
- [18] W. T. Read and W. Shockley, *Phys. Rev.* **78**, 275 (1950).
- [19] L. E. Murr, *Interfacial Phenomena in Metals and Alloys* (Adison Wesley, New York, 1975).
- [20] J.-M. Zhang, Y.-H. Huang, X.-J. Wu, and K.-W. Xu, *Appl. Surf. Sci.* **252**, 4936 (2006).